Available online at www.sciencedirect.com

ScienceDirect

Procedia Engineering 00 (2016) 000–000

Procedia Engineering

www.elsevier.com/locate/procedia

Modern Building Materials, Structures and Techniques, MBMST 2016

Peridynamic mesh sensitivity analysis for quasi-static simulations

Andris Freimanis*, Ainars Paeglitis

Institute of Transportation Engineering, Riga Technical University, Kipsalas iela 6A, Riga, LV1048, Latvia

Abstract

Peridynamics is a non-local formulation of continuum mechanics that doesn't rely on spatial derivatives, therefore peridynamics is well suited for crack and failure modeling. A body is discretized in a finite number of particles and each particle connects to other particles within a range called a material's horizon. In this study we ran fifty simulations with different horizon size and particle spacing combinations to see how they influence maximum displacement. Values from simulations are compared with values calculated using Hooke's law. The results show that the horizon size of three particle spacings gives the best results. However, simulations with horizon sizes non-integer times larger than particle spacing show unexpectedly good results.

Peer-review under responsibility of the organizing committee of MBMST 2016.

Keywords: Peridynamics; mesh; convergence; sensitivity; state-based

1. Introduction

Peridynamic theory [1] is a nonlocal formulation of continuum mechanics that was created to handle materials' discontinuities such as cracks. Classical theory relies on spatial derivatives to represent the relative displacement and force between two particles and partial derivatives with respect to the spatial coordinates are undefined along the discontinuities. In contrast, peridynamics (PD) uses integral equations that do not require spatial derivatives. PD was first introduced in the bond-based form [2], in which Poisson's ratio is limited to 0.25. In 2007 Silling et al. [3] introduced the state-based formulation that eliminated this restriction. A PD body is discretized in a number of particles each of which describes some amount of volume and the side of a particle is commonly called a lattice. The results depend on particle positions, particle spacing h, and material's horizon δ (see chapter 2 for PD theory). Most common are square lattices for two-dimensional analysis and cubic lattices for three-dimensional analysis both with

* Corresponding author. Tel.: +371 263 823 52;
E-mail address: andris.freimanis_1@edu.rtu.lv

Peer-review under responsibility of the organizing committee of MBMST 2016.

uniform spacing in all directions [5, 9–12] . PD have been used successfully to predict damage and failure [4–8], however, few articles deal with the mesh spacing's and horizon's influence on the results.

Given a domain of m discretized particles with h being the distance between two neighboring particles, Bobaru et al. defined three convergence types in [13]:

- h – convergence, where δ is fixed as $h \to 0$;
- (δh) – convergence, where δ decreases and h decreases, but the ratio between them stays the same;
- δ – convergence, where $\delta \to 0$ with a fixed h.

Yaghoobi and Chorzepa considered (δh) and δ convergence types for a two-dimensional mesh in [6] and found that the results are the most accurate with $\delta/h = 3.015$. In [4] Silling and Askari used four mesh spacings to show how crack growth changes based on the mesh spacing in a two-dimensional plate. Study [14] showed that in two-dimensional plate with a crack the difference in displacements between PD and finite-element method (FEM) shrinks as δ decreases. Henke and Shanbhag [15] found that cubic mesh with $\delta/h = 4$ gives better results than meshes with lower δ/h value, however, centroidal Voronoi tessellation mesh gives similar or better results. In [16] δ convergence and h convergence studies were performed for unidirectional composites. Previously mentioned studies (with the exception of [15]) used two-dimensional models for their analysis.

For this study, we simulated a tensile and a compression test of glass-fiber coupons in three-dimensions. Simulated displacement values are compared with displacement values obtained from Hooke's law and percent errors are calculated. We use different h and δ values to study five cases of δ and five cases of (δh) convergence.

2. Peridynamic theory

In PD an undeformed body consists of an infinite number of particles identified by their coordinates, $\mathbf{x}_{(i)}$. Each particle is associated with some amount of volume $V_{(i)}$. These particles undergo displacement $\mathbf{u}_{(i)}$ and their position in the deformed configuration is described by the position vector $\mathbf{y}_{(i)}$. Each particle has a range $\delta > 0$ called the "horizon", named so because the particle can't "see" past it. In three-dimensional space particles within a sphere, with a radius of δ and centered at particle $\mathbf{x}_{(i)}$, are called the family of $\mathbf{x}_{(i)}$, $H_{\mathbf{x}_{(i)}}$. An example of peridynamic body is shown in Fig. 1. Particle $\mathbf{x}_{(i)}$ interacts through bonds $\langle \mathbf{x}_{(j)} - \mathbf{x}_{(i)} \rangle$ with all particles in its family and the bond properties depend on material models. The force density vector, which can be viewed as the force exerted by particle $\mathbf{x}_{(i)}$ on the particle $\mathbf{x}_{(j)}$, is then $\mathbf{t}_{(i)(j)}$. Similarly particle $\mathbf{x}_{(i)}$ is influenced by $\mathbf{x}_{(j)}$ through the force density vector $\mathbf{t}_{(j)(i)}$. These forces are determined jointly by the collective deformation of neighborhoods $H_{\mathbf{x}_{(i)}}$ and $H_{\mathbf{x}_{(j)}}$ throughout the model. Force density vectors $\mathbf{t}_{(i)(j)}$ where $(j = 1,2,...,\infty)$ associated with particle $\mathbf{x}_{(i)}$ are stored in infinite-dimensional array, called a force vector state, $\underline{\mathbf{T}}$ (1) and the relative position vectors in the deformed configuration $(\mathbf{y}_{(j)} - \mathbf{y}_{(i)})$ where $(j = 1,2,...,\infty)$ can be stored in an similar array called a deformation vector state, $\underline{\mathbf{Y}}$ (2).

$$\underline{\mathbf{T}}(\mathbf{x}_{(i)}, t) = \begin{Bmatrix} \mathbf{t}_{(i)(1)} \\ \vdots \\ \mathbf{t}_{(i)(\infty)} \end{Bmatrix}, \tag{1}$$

$$\underline{\mathbf{Y}}(\mathbf{x}_{(i)}, t) = \begin{Bmatrix} (\mathbf{y}_{(1)} - \mathbf{y}_{(i)}) \\ \vdots \\ (\mathbf{y}_{(\infty)} - \mathbf{y}_{(i)}) \end{Bmatrix} \tag{2}$$

Force vector state for particle $\mathbf{x}_{(i)}$ depends on the relative displacements between that particle and all other particles within its horizon, therefore force vector state can also be written as

$$\underline{\mathbf{T}}(\mathbf{x}_{(i)}, t) = \underline{\mathbf{T}}(\underline{\mathbf{Y}}(\mathbf{x}_{(i)}, t)).$$

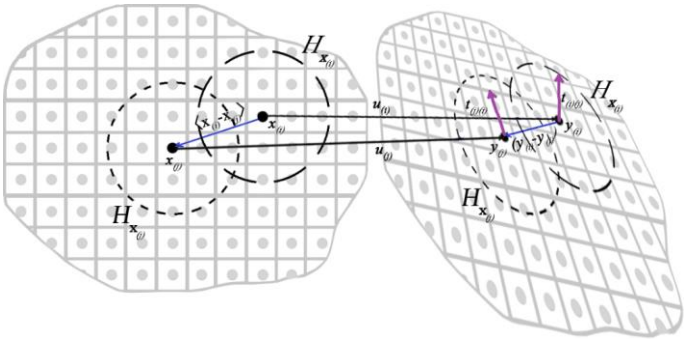

Fig. 1. Peridynamic body before deformation (left) and after deformation (right).

Force density vector $\mathbf{t}_{(i)(j)}$ and position vector $(\mathbf{y}_{(j)} - \mathbf{y}_{(i)})$ between two particles $\mathbf{x}_{(i)}$ and $\mathbf{x}_{(j)}$ can be expressed as

$$\mathbf{t}_{(i)(j)}(\mathbf{u}_{(j)} - \mathbf{u}_{(i)}, \mathbf{x}_{(j)} - \mathbf{x}_{(i)}, t) = \underline{\mathbf{T}}(\mathbf{x}_{(i)}, t)\left\langle \mathbf{x}_{(j)} - \mathbf{x}_{(i)} \right\rangle$$
$$(\mathbf{y}_{(j)} - \mathbf{y}_{(i)}) = \underline{\mathbf{Y}}(\mathbf{x}_{(i)}, t)\left\langle \mathbf{x}_{(j)} - \mathbf{x}_{(i)} \right\rangle$$

The PD equation of motion in integral form is:

$$\rho(\mathbf{x}_{(i)})\ddot{\mathbf{u}}(\mathbf{x}_{(i)}, t) = \int_H \left(\underline{\mathbf{T}}(\mathbf{x}_{(i)}, t)\left\langle \mathbf{x}_{(j)} - \mathbf{x}_{(i)} \right\rangle - \underline{\mathbf{T}}(\mathbf{x}_{(j)}, t)\left\langle \mathbf{x}_{(i)} - \mathbf{x}_{(j)} \right\rangle \right) dH + \mathbf{b}(\mathbf{x}_{(i)}, t) ,$$

where $\rho(\mathbf{x}_{(i)})$ - density of a particle, $\ddot{\mathbf{u}}(\mathbf{x}_{(i)}, t)$ - acceleration vector, $\mathbf{b}(\mathbf{x}_{(i)}, t)$ - body load density vector. Damage and failure in PD is modeled through breaking of bonds. When a bond is broken the load it carried is redistributed among the unbroken bonds, leading to progressive damage and failure. The simplest damage model is the critical stretch i.e. a bond is irreversibly broken when it is stretched past some value. We didn't use any damage models for this study so they won't be discussed further, but [4] describes them in more detail. In this paper we use isotropic linear peridynamic solid (LPS) material model, which is the nonlocal analogue to a classical linear elastic isotropic material model, additional details are given in [3]. The isotropic LPS model has a force scalar state:

$$\underline{t} = \frac{3K\theta}{m}\underline{\omega}\underline{x} + \frac{15\mu}{m}\underline{\omega}\underline{e}^d$$

where $\underline{t}$ - force scalar state, K - bulk modulus, m - weighted volume, $\underline{x}$ - reference position scalar state, μ - shear modulus, $\underline{\omega}$ - influence function (equal to 1 for isotropic materials), $\underline{e}^d$ - deviatoric part of extension scalar state.

3. Specimens and simulations

3.1. Specimens

One tensile and one compression specimen was randomly selected from a batch of tested four-layer twintex specimens made from polypropylene glass comingled fabric using vacuum consolidation. They were incrementally loaded till failure either in tension or compression. Applied load was measured by testing machine itself, but strain was measured by IMETRUM digital image correlation (DIC) system. Tensile test was done according to ASTM D 3039 standard, tensile modulus of elasticity was calculated between 0.001 and 0.003 strain, Poison's ratio was taken as average between values at 20% and 30% of failure load. Compression test was done according to ASTM D 3410 standard and compression modulus of elasticity was calculated between 0.001 and 0.003 strain. Poisson's ratio for compression simulation was taken from the tensile test. For simplicity, the tensile specimen will hereafter be called

specimen T and the compression specimen will be called specimen C. Specimen width, thickness, cross-sectional area, failure load, and other measurements are given in table 1, since specimens were clamped at both ends the length values in table 1. show specimens' length between these two clamps.

Table 1. Specimen data from tensile and compression test.

Specimen	Thickness (mm)	Width (mm)	Length (mm)	Failure load (N)	Modulus of elasticity (GPa)	Poisson's ratio	Density (kg/m^3)
T	2.10	15.73	100.00	8598.35	12.13	0.36	1240.00
C	2.00	10.57	10.00	3209.58	13.91	0.36	1240.00

3.2. Discretization

To run a simulation, it is necessary to discretize a body in a finite number of particles. The distance between two neighboring particles is equal to the lattice in the direction of the neighboring particle because all particles have the same size. Specimens' side length ratio is not an integer number, so it was impossible to fit an integer number of cubic particles in a specimens' volume. To address this, we calculated the largest lattice by dividing specimens' thickness into an integer number of particles, then reduced the calculated lattice size to fit an integer number of particles in specimens' length and width. Five different mesh densities are considered here by making the largest lattices equal to thickness divided by either one two, three, four or five. The lowest limit of thickness division was one, so a two dimensional model for 10 simulations, and five was chosen as the highest limit, as finer meshes increased computational cost too much. Because of this approach, the particles weren't a perfect cube, with the largest difference between two sides of a particle being 6.37% for specimen T and 11.92% for specimen C.

To study δ convergence, the horizon has to shrink as the spacing between the particles remains constant. In a discretized body δ must not be lower than spacing between the particles, otherwise a particle won't be connected to other particles. For this study, we considered horizons with sizes from one largest particle spacing to five largest particle spacings, larger sizes weren't considered due to increasing computational cost. It is recommended in [17] to increase the horizon by some small number to avoid excluding any particles from a family due to a floating point error, so we increased all horizons by one percent. A total of 25 different cases for each specimen are considered here. For clarity, cases will be labeled as Lmn, where L is the name of the specimen (T or C), m is the number of particles in specimen's thickness (1 to 5) and n is the size of the horizon in lattices (1 to 5). Particle and horizon sizes are given in Table 2.

Table 2. Particle and horizon size for all considered cases (cases with a * have an increased horizon, see chapter 3.3).

Case	δ (m)	hx (m)	hy (m)	hz (m)	Case	δ (m)	hx (m)	hy (m)	hz (m)
T1n	(1 ... 5)×1.01×h_y	0.002097	0.0021	0.001966	C11*	0.002692	0.002	0.002	0.001762
					C1n	(2 ... 5)×1.01×h_y	0.002	0.002	0.001762
T2n	(1 ... 5)×1.01×h_y	0.001048	0.00105	0.001049	C21*	0.001428	0.001	0.001	0.000961
					C2n	(2 ... 5)×1.01×h_y	0.001	0.001	0.000961
T3n	(1 ... 5)×1.01×h_y	0.000699	0.0007	0.000684	C31*	0.000949	0.000662	0.000667	0.000661
					C3n	(2 ... 5)×1.01×h_y	0.000662	0.000667	0.000661
T4n	(1 ... 5)×1.01×h_y	0.000524	0.000525	0.000524	C41*	0.000714	0.0005	0.0005	0.00048
					C4n	(2 ... 5)×1.01×h_y	0.0005	0.0005	0.00048
T5n	(1 ... 5)×1.01×h_y	0.000419	0.00042	0.000414	C51*	0.000573	0.0004	0.0004	0.000391
					C5n	(2 ... 5)×1.01×h_y	0.0004	0.0004	0.000391

3.3. Loads, boundary conditions and simulations

In PD loads and boundary conditions are prescribed to some amount of volume. Because of this, three rows of particles were added to each end of both specimens bringing specimen's T total length to 100mm+ $6h_x$ and specimen's C total length to 10 mm+ $6h_x$, these added rows will be called boundary regions. The boundary region at one end was constrained in all directions, but at the other end the only in y and z directions and the load was applied in the x direction. Since load is applied to some volume it has to be force per unit volume. Table 3. shows the number of particles in a single boundary region, the volume of a single particle, and the applied load per unit volume per particle. Maximum applied load is showed in table 2.

Table 3. Number of particles with a prescribed boundary condition at one end, single particle's volume and the load per unit volume applied to a single particle.

Case	Number of particles in a single boundary region	Particle's volume (m^3)	Load applied to a single particle (N/m^3)	Case	Number of particles in a single boundary region	Particle's volume (m^3)	Load applied to a single particle (N/m^3)
T1n	24	$8.66e^{-9}$	$4.14e^{+10}$	C1n	18	$7.05e^{-9}$	$-2.53e^{+10}$
T2n	90	$1.15e^{-9}$	$8.28e^{+10}$	C2n	66	$9.61e^{-10}$	$-5.06e^{+10}$
T3n	207	$3.35e^{-10}$	$1.24e^{+11}$	C3n	144	$2.92e^{-10}$	$-7.65e^{+10}$
T4n	360	$1.44e^{-10}$	$1.66e^{+11}$	C4n	264	$1.20e^{-10}$	$-1.01e^{+11}$
T5n	570	$7.29e^{-11}$	$2.07e^{+11}$	C5n	405	$6.26e^{-11}$	$-1.27e^{+11}$

Simulations were done with Peridigm software [17]. Specimens were modeled using state-based elastic material model described in [3] with the material properties given in Table 1. Quasi-static solver applied the load incrementally in 50 load steps and the tolerance criteria was set to $1.0e^{-3}$. Maximum displacement values from PD solution were compared to values calculated using Hooke's law (3).

$$d = l\frac{F}{AE} \tag{3}$$

, where d - absolute displacement, l - specimen's length, F - applied load, A - cross-sectional area, E - modulus of elasticity. The comparison was done using percent error.

Simulations of five compression cases with $\delta = 1h$ (Cm1) wouldn't converge when 50 loads steps were used, nor when the number of load steps was increased to $1e^{+6}$. In these cases a particle is connected only to its immediate neighbors. The convergence doesn't seem to be dependent on the particle spacing, because this issue occurred with all mesh sizes. We decided to increase the horizon for these five cases to include not only the immediate neighbors, but also the next layer of particles. This increase changed δ from $\delta = 1h$ to about $\delta = 1.4h$, but we didn't change the case naming scheme, two-dimensional case is illustrated in fig. 2 and table 2 shows the increased horizons.

4. Results and discussion

In this study we ran 50 simulations with parameters described in tables 1, 2, and 3. Percent errors between maximum displacements from simulations and displacements calculated using (3) were used to study five cases of δ convergence and five cases of (δh) convergence. Displacement values from Hooke's law (3) at maximum load were $2.14e^{-3}$ m for specimen T and $-1.09e^{-4}$ m for specimen C. Maximum displacement values from simulations are shown in table 4 and percent errors in table 5. T53 is the most accurate simulation case in tension and C43 is the most accurate in compression. The two-dimensional cases (T1n and C1n) are less accurate than three-dimensional cases, when δ sizes with similar ratios to h are compared. It can be seen that every simulation underestimated the displacement when compared to Hooke's law in both tension and compression. Generally coarser mesh results in larger difference from Hooke's law, but it also varies with changing horizon, differences are better illustrated in the following figures. In the following figures values calculated using Hooke's law are denoted HL.

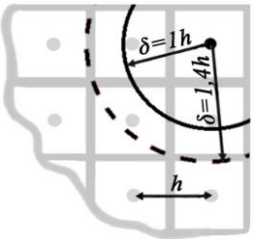

Fig. 2. Initial and updated horizon sizes for a two-dimensional case.

Error dependence on changes in the horizon size δ as the lattice size stays constant (δ convergence) is shown in Fig. 4. In tension, the two-dimensional cases (T1n) show the worst results and, as expected, the results from three-dimensional cases increase in accuracy as particle density increases. In compression two-dimensional cases (C1n) still show the worst results, but the accuracy no longer increases with increasing particle density. The C43 case shows the lowest error, followed by C31case, and only then followed by C53 case. This shows that in compression finer mesh doesn't always lead to more accurate results. The best results in tension are obtained with the horizon size three times larger than the lattice and deviations only leads to less accurate results. Compression simulations with $\delta = 1h$ wouldn't converge, so the horizon size for these cases was increased to about $\delta = 1.4h$, which lead to unexpected decrease in calculated percent errors. For C1n and C2n cases this horizon size showed the most accurate results, for C3n – C5n cases the accuracy was within 5% from $\delta = 3h$ cases. We don't know why there was such an increase, but it might indicate that better accuracy can be achieved by using horizon sizes that are not equal to lattice length multiplied by some integer number. The graphs of compression cases intersect, which means that, for different horizon sizes, different mesh densities are the most accurate. This might be caused by the fact that particles aren't completely cubic, but it should be additionally tested.

Table 4. Maximum displacement values (m) for all simulation cases.

δ	Specimen T					Specimen C				
	h					h				
	1	2	3	4	5	1	2	3	4	5
1	5.67e-04	8.07e-04	8.62e-04	9.02e-04	9.19e-04	-1.72e-05	-2.80e-05	-3.02e-05	-2.94e-05	-2.80e-05
2	6.17e-04	1.25e-03	1.40e-03	1.54e-03	1.58e-03	-1.13e-05	-2.08e-05	-2.40e-05	-2.43e-05	-2.35e-05
3	9.32e-04	1.35e-03	1.72e-03	2.00e-03	2.07e-03	-1.53e-05	-2.15e-05	-2.91e-05	-3.11e-05	-3.01e-05
4	8.10e-04	1.18e-03	1.48e-03	1.63e-03	1.75e-03	-1.35e-05	-2.07e-05	-2.31e-05	-2.84e-05	-2.57e-05
5	6.78e-04	1.10e-03	1.38e-03	1.49e-03	1.74e-03	-1.21e-05	-1.97e-05	-2.10e-05	-2.54e-05	-2.60e-05

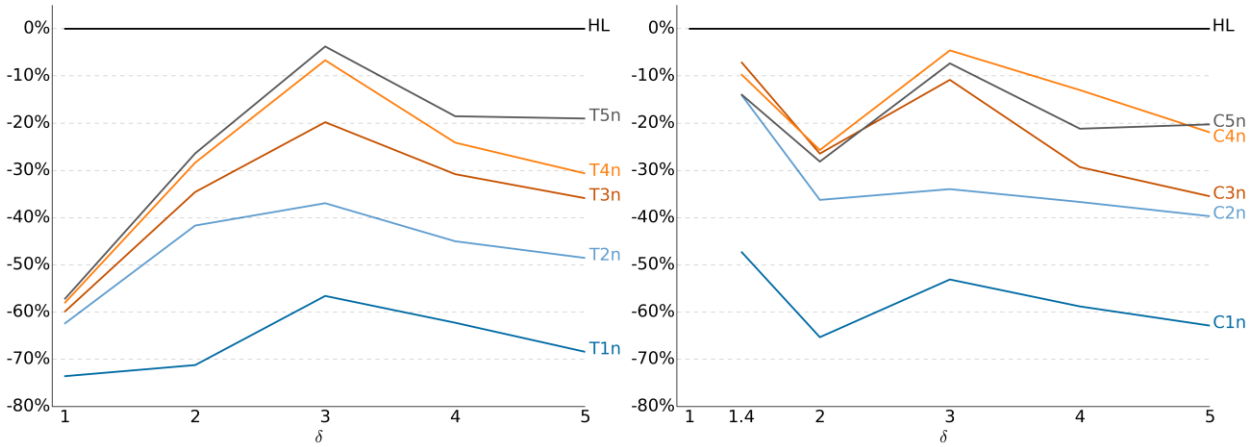

Fig. 4. Percent error vs. horizon size (δ convergence) graphs for tension specimen (left) and compression specimen (right).

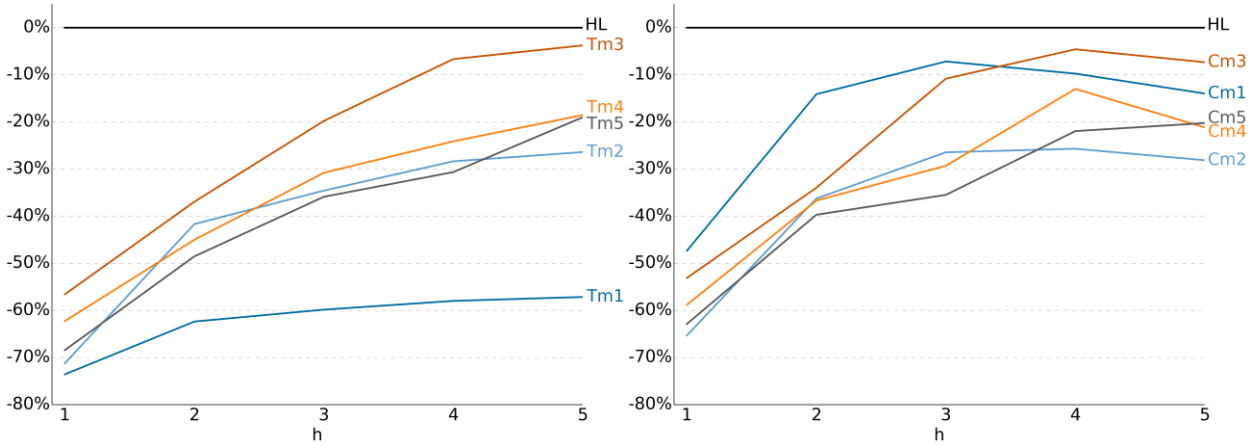

Fig. 5. Percent error vs. particle spacing ((δh) convergence) graphs for tension specimen (left) and compression specimen (right).

Table 5. Percent errors between maximum displacements from simulations and Hooke's law.

δ	Specimen T					Specimen C				
	h					h				
	1	2	3	4	5	1	2	3	4	5
1	-73.57%	-62.37%	-59.85%	-57.99%	-57.15%	-47.34%	-14.12%	-7.18%	-9.76%	-13.98%
2	-71.23%	-41.68%	-34.58%	-28.37%	-26.41%	-65.32%	-36.25%	-26.45%	-25.70%	-28.14%
3	-56.59%	-36.95%	-19.80%	-6.68%	-3.76%	-53.10%	-33.97%	-10.83%	-4.59%	-7.34%
4	-62.27%	-45.01%	-30.80%	-24.13%	-18.54%	-58.80%	-36.69%	-29.31%	-13.00%	-21.18%
5	-68.43%	-48.54%	-35.89%	-30.65%	-19.02%	-62.87%	-39.71%	-35.49%	-21.96%	-20.26%

Fig. 5 shows (δh) convergence, namely, how percent error changes as the horizon size δ and the lattice size h decreases while the ratio between them stays the same. For tension specimens errors decreases with a decrease in lattice size. Errors are largest when particles are only connected to their immediate neighbors $\delta/h = 1$ and the most accurate when $\delta/h = 3$. The results for compression cases are less clear. Since the simulations with $\delta/h = 1$ wouldn't converge, δ was increased to about $1.4h$ (these cases are still named Cm1). The results show that in compression the simulations with $\delta/h = 1.4$ are the most accurate for larger lattices e.g. $h = 1\text{-}3$, but as mesh density increases further, cases with $\delta/h = 3$ become more accurate. However, cases with $\delta/h = 1.4$ still show better results than cases with other ratios.

5. Conclusions

In this paper we analyze the influence of the horizon size and mesh spacing on the results of peridynamic simulations. Twenty five tension and twenty five compression cases with different mesh spacing and horizon sizes are considered. Glass fiber coupon tests were used to determine input values for simulations and Peridigm software was used to run the simulations. The results showed that two-dimensional cases are less accurate than three-dimensional cases if similar horizon size to lattice size ratio is considered.

δ convergence study showed that most accurate results are obtained when the horizon size is three times larger than the lattice and further increase in the horizon size leads to decrease in accuracy. Five compression cases with a horizon size of $1.4h$ showed similar or better results than cases with larger horizon sizes. This could indicate that more

accurate results can be obtained using horizon sizes that are not equal to the lattice size multiplied by some integer number, however, additional studies are required.

(δh) convergence study showed that in tension even with changing lattice size the horizon to lattice size ratio of three gives the most accurate results. In compression the horizon size of $1.4h$ is the most accurate for higher particle spacing, but the horizon size of three lattices gives more accurate results when particle spacing decreases.

Additionally lines in δ and (δh) convergence graphs intersected, which shows that a constant change in the horizon size or lattice length doesn't change the accuracy by constant amount. This, however, could be caused by the fact that particles weren't perfect cubes.

Acknowledgements

The research leading to these results has received the funding from Latvia State Research Programme under grant agreement "Innovative materials and smart technologies for environmental safety, IMATEH".

References

[1] E. Madenci and E. Oterkus, *Peridynamic Theory and Its Applications*. New York, NY: Springer New York, 2014.
[2] S. A. Silling, "Reformulation of elasticity theory for discontinuities and long-range forces," *J. Mech. Phys. Solids*, vol. 48, no. 1, pp. 175–209, 2000.
[3] S. A. Silling, M. Epton, O. Weckner, J. Xu, and E. Askari, "Peridynamic states and constitutive modeling," *J. Elast.*, vol. 88, no. 2, pp. 151–184, 2007.
[4] S. A. Silling and E. Askari, "A meshfree method based on the peridynamic model of solid mechanics," *Comput. Struct.*, vol. 83, no. 17–18, pp. 1526–1535, 2005.
[5] E. Madenci and S. Oterkus, "Ordinary state-based peridynamics for plastic deformation according to von Mises yield criteria with isotropic hardening," *J. Mech. Phys. Solids*, vol. 86, pp. 192–219, 2016.
[6] A. Yaghoobi and M. G. Chorzepa, "Meshless modeling framework for fiber reinforced concrete structures," *Comput. Struct.*, vol. 161, pp. 43–54, 2015.
[7] C. Sun and Z. Huang, "Peridynamic simulation to impacting damage in composite laminate," *Compos. Struct.*, vol. 138, pp. 335–341, 2016.
[8] P. Perré, G. Almeida, M. Ayouz, and X. Frank, "New modelling approaches to predict wood properties from its cellular structure: image-based representation and meshless methods," *Ann. For. Sci.*, 2015.
[9] E. Oterkus, E. Madenci, O. Weckner, S. Silling, P. Bogert, and A. Tessler, "Combined finite element and peridynamic analyses for predicting failure in a stiffened composite curved panel with a central slot," *Compos. Struct.*, vol. 94, no. 3, pp. 839–850, 2012.
[10] D. Huang, G. Lu, and P. Qiao, "An improved peridynamic approach for quasi-static elastic deformation and brittle fracture analysis," *Int. J. Mech. Sci.*, vol. 94–95, pp. 111–122, 2015.
[11] Q. Zhang, X. Gu, and D. Huang, "Failure analysis of plate with non-uniform arrangement holes by ordinary state-based peridynamics," 2015, no. July, pp. 0–10.
[12] A. Askari, Y. Azdoud, F. Han, G. Lubineau, and S. Silling, "Peridynamics for analysis of failure in advanced composite materials," *Numer. Model. Fail. Adv. Compos. Mater.*, no. AUGUST, pp. 331–350, 2015.
[13] F. Bobaru, M. Yang, L. F. Alves, S. A. Silling, E. Askari, and J. Xu, "Convergence, adaptive refinement, and scaling in 1D peridynamics," *Int. J. Numer. Methods Eng.*, vol. 77, no. 6, pp. 852–877, Feb. 2009.
[14] W. Hu, Y. D. Ha, F. Bobaru, and S. A. Silling, "The formulation and computation of the nonlocal J-integral in bond-based peridynamics," *Int. J. Fract.*, vol. 176, no. 2, pp. 195–206, 2012.
[15] S. F. Henke and S. Shanbhag, "Mesh sensitivity in peridynamic simulations," *Comput. Phys. Commun.*, vol. 185, no. 1, pp. 181–193, 2014.
[16] W. Hu, Y. D. Ha, and F. Bobaru, "Peridynamic model for dynamic fracture in unidirectional fiber-reinforced composites," *Comput. Methods Appl. Mech. Eng.*, vol. 217–220, pp. 247–261, 2012.
[17] M. L. Parks, D. J. Littlewood, J. a Mitchell, and S. a Silling, "Peridigm Users ' Guide," 2012.